THE JOURNAL OF BIOLOGICAL CHEMISTRY VOL. 285, NO. 36, pp. 27536–27544, September 3, 2010

Escherichia coli Cell Surface Perturbation and Disruption Induced by Antimicrobial Peptides BP100 and pepR*

Received for publication, April 6, 2010, and in revised form, May 21, 2010 Published, JBC Papers in Press, June 21, 2010, DOI 10.1074/jbc.M110.130955

Carla S. Alves[‡], Manuel N. Melo[§], Henri G. Franquelim[§], Rafael Ferre[¶], Marta Planas[¶], Lidia Feliu[¶], Eduard Bardají[¶], Wioleta Kowalczyk[‖1], David Andreu[‖], Nuno C. Santos[§], Miguel X. Fernandes[‡], and Miguel A. R. B. Castanho[§2]

From the [‡]Centro de Química da Madeira, Universidade da Madeira, Campus Universitário da Penteada, 9000-390 Funchal, Portugal, the [§]Instituto de Medicina Molecular, Faculdade de Medicina, Universidade de Lisboa, 1649-028 Lisbon, Portugal, the [¶]Laboratori d'Innovació en Processos i Productes de Síntesi Orgànica, Departament de Química, Universitat de Girona, Campus Montilivi, 17071 Girona, Spain, and the [‖]Department of Experimental and Health Sciences, Pompeu Fabra University, Barcelona Biomedical Research Park, E-08003 Barcelona, Spain

The potential of antimicrobial peptides (AMPs) as an alternative to conventional therapies is well recognized. Insights into the biological and biophysical properties of AMPs are thus key to understanding their mode of action. In this study, the mechanisms adopted by two AMPs in disrupting the Gram-negative *Escherichia coli* bacterial envelope were explored. BP100 is a short cecropin A-melittin hybrid peptide known to inhibit the growth of phytopathogenic Gram-negative bacteria. pepR, on the other hand, is a novel AMP derived from the dengue virus capsid protein. Both BP100 and pepR were found to inhibit the growth of *E. coli* at micromolar concentrations. Zeta potential measurements of *E. coli* incubated with increasing peptide concentrations allowed for the establishment of a correlation between the minimal inhibitory concentration (MIC) of each AMP and membrane surface charge neutralization. While a neutralization-mediated killing mechanism adopted by either AMP is not necessarily implied, the hypothesis that surface neutralization occurs close to MIC values was confirmed. Atomic force microscopy (AFM) was then employed to visualize the structural effect of the interaction of each AMP with the *E. coli* cell envelope. At their MICs, BP100 and pepR progressively destroyed the bacterial envelope, with extensive damage already occurring 2 h after peptide addition to the bacteria. A similar effect was observed for each AMP in the concentration-dependent studies. At peptide concentrations below MIC values, only minor disruptions of the bacterial surface occurred.

Antimicrobial peptides (AMPs)[3] represent a group of naturally occurring molecules that play a key role in the innate defense system of virtually all organisms (1). Their robust mode of action (2, 3), as well as their broad activity toward bacteria, fungi, protozoa, and viruses (1, 4), makes AMPs appealing candidates for the development of new and more efficient antimicrobial agents. In fact, they provide an alternative to conventional antibiotics for the treatment of resistant pathogens (2, 3). An understanding of the mechanisms adopted by the AMPs is thus central to the advancement of these molecules to the status of a new group of broad-spectrum antimicrobial agents.

Characterization of AMPs has revealed a highly heterogeneous group of molecules, which differ in sequence, length, and structural conformation (α-helical, β-sheet, extended, and looped) (3, 5). Despite these variations, two functionally important features are shared by most AMPs: a net positive charge and the ability to adopt an amphipathic structure. The net positive charge allows for the electrostatic binding of the peptide to the anionic microbial surface, while the amphipathic structure promotes peptide insertion into the hydrophobic core of the cell membrane (2, 3). Several models describing membrane disruption as a result of these direct peptide-lipid interactions have been proposed: the barrel-stave pore model (6, 7), the toroidal pore model (6–9), the disordered toroidal pore model (7, 10), and the carpet model (7, 9, 11). Regardless of the mechanism adopted, a threshold peptide concentration needs to be reached for disruption of the membrane structure to occur (6, 7). Alternative mechanisms involving cytoplasmic invasion and interference of core metabolic functions have also been considered to account for the antimicrobial properties of some AMPs (2). In these cases, the microbial outer membrane must still be traversed to allow peptide penetration into the cell. Analysis of the peptide interactions at the membrane level is therefore central to the understanding of the mode of action of AMPs.

In this study, the modes of action of two distinctly different AMPs on the cell envelope of *E. coli* are explored. The first peptide, BP100 (KKLFKKILKYL-NH_2), is a short cationic cecropin A-melittin hybrid (12) obtained through a combinatorial chemistry approach (13). It has been established as an effective AMP, capable of inhibiting *in vitro* the growth of the economically important plant pathogenic Gram-negative bacteria *Erwinia amylovora*, *Pseudomonas syringae* pv. *Syringae*, and *Xanthomonas axonopodis* pv. *vesicatoria*, as well as *in vivo* the growth of *E. amylovora* (13). BP100 has also been reported to display minimal cytotoxicity and low susceptibility to proteinase K degradation (13). Details of the membrane perturbation mechanisms adopted by this peptide

* This work was supported by the Fundação para Ciência e Tecnologia, Portugal (Fellowships SFRH/BD/24547/2005, SFRH/BD/24778/2005, and SFRH/BD/39039/2007, to C. S. A., M. N. M., and H. G. F., respectively, and Projects PTDC/QUI/69937/2006 and REEQ/140/BIO/2005).

[1] Fellow in the Juan de la Cierva Program of the Spanish Ministry of Science and Innovation.

[2] To whom correspondence should be addressed: Unidade Bioquímica Física, Instituto de Medicina Molecular, Faculdade de Medicina da Universidade de Lisboa, Av. Professor Egas Moniz, 1649-028, Lisboa, Portugal. Tel.: 351-217985136; Fax: 351-217999477; E-mail: macastanho@fm.ul.pt.

[3] The abbreviations used are: AMP, antimicrobial peptide; MIC, minimal inhibitory concentration; AFM, atomic force microscopy; MHB, Mueller Hinton Broth; PLL, poly-L-lysine.

have largely been revealed through biophysical studies (14). A strong selectivity toward anionic bacterial membrane models was detected for BP100, with a strong correlation between the closely coupled processes of charge neutralization, permeabilization, and translocation being identified. The second peptide, pepR (LKRWGTIKKSKAINVLRGFRKEIGRMLNILNRRRR), is derived from the putative RNA-binding domain of the dengue virus capsid protein (15). The structural features of this peptide as observed in the capsid protein (*i.e.* cationic, amphipathic α-helix) seem to point to a potentially potent AMP.

Here, we present the characterization of BP100 and pepR effects toward *E. coli*, both at cellular and molecular levels. Antimicrobial susceptibility and surface charge studies were used to explore the concept of a neutralization-mediated killing mechanism adopted by either AMP. In addition to this, AFM was used to assess the bactericidal effect of each AMP on the cell envelope morphology of *E. coli*, a representative Gram-negative bacterium. It is worth stressing that both peptides are not effective against Gram-positive bacteria, for which other considerations may apply.

EXPERIMENTAL PROCEDURES

Peptide Syntheses—BP100 and pepR were synthesized as C-terminal carboxamides on Rink amide MBHA resin (Novabiochem, Läufelfingen, Switzerland) using standard 9-fluorenylmethyloxycarbonyl (Fmoc) solid-phase synthesis methods (13, 16) in a model 433 automated synthesizer (Applied Biosystems, Foster City, CA) running FastMoc protocols. After deprotection and cleavage with trifluoroacetic acid/water/ethanedithiol/triisopropylsilane (94:2.5:2.5:1, v/v, 90 min, 25 °C), the peptides were isolated by precipitation with chilled diethyl ether, taken up in aqueous acetic acid and lyophilized. The synthetic material was purified to >95% homogeneity by reverse-phase HPLC and further characterized for identity by electrospray or MALDI-TOF mass spectrometry.

Preparation of Bacterial Cells—E. coli (ATCC 25922), maintained as stock cultures at −80 °C, were revived by growing on Luria-Bertani agar (Laboratorios CONDA, Madrid, Spain) plates overnight at 37 °C. An isolated bacterial colony was used to inoculate Mueller Hinton Broth (MHB; OXOID LTD, Hampshire, England), and the bacterial culture was allowed to grow overnight at 37 °C. A 100-μl volume of the culture was used to freshly inoculate 5 ml of MHB. The suspension was then allowed to grow at 37 °C for 105 min, where a final bacterial concentration of $\sim 3 \times 10^8$ colony-forming units/ml (cfu/ml) was reached ($A_{600} \sim 0.1$). Bacterial suspensions were diluted using fresh MHB to 3×10^5 cfu/ml for the antimicrobial activity and zeta potential studies, and to 3×10^6 cfu/ml for the AFM imaging experiments. For the latter two methodologies, cells were centrifuged at 11,400 × *g* for 8 min, and washed twice under the same conditions using 10 mM HEPES buffer, pH 7.4, containing 150 mM NaCl.

Antimicrobial Susceptibility Assay—The antimicrobial activities of BP100 and pepR against *E. coli* were monitored using a slightly modified microtiter broth dilution method (17). In brief, the lyophilized peptides were solubilized in sterile Milli-Q water to a final concentration of 1 mM and filter sterilized using a 0.22-μm pore size filter. Dilutions of the synthetic peptides were then prepared to obtain final concentrations of 5, 10, 20, 40, and 80 μM for BP100, and of 6.3, 12.5, 25, 50, 100, and 200 μM for pepR. Each dilution (11.1 μl) was dispensed into a polypropylene microtiter plate well already containing 100 μl of the prepared 3×10^5 cfu/ml *E. coli* inoculum. Final peptide concentrations of 0.5, 1, 2, 4, and 8 μM were tested for BP100, and 0.63, 1.25, 2.5, 5, 10, and 20 μM for pepR. Two replicates were performed for each peptide and concentration used. Positive controls contained filter-sterilized Milli-Q water instead of peptide. The plate was incubated for 18 h at 37 °C without shaking. The growth of the bacterial suspension in each well was then quantified by A_{600} measurement. The lowest peptide concentration to inhibit >50% growth was defined as the minimal inhibitory concentration (MIC). The experiment was repeated twice.

Surface Charge Measurements—The zeta potential studies were performed at 25 °C on a Zetasizer Nano ZS (Malvern Instruments, Worcestershire, UK) equipped with a 633-nm HeNe laser. Dilutions of the synthetic peptides were prepared to final concentrations of 5, 10, 20, 40, and 80 μM for BP100, and of 6.3, 12.5, 25, 50, 100, and 200 μM for pepR using 10 mM HEPES buffer, pH 7.4, containing 150 mM NaCl, and then filtered using a 0.22-μm pore-size filter. A 100-μl volume of each peptide stock dilution was added to 900 μl of the *E. coli* cells. Positive controls contained filtered buffer instead of peptide. The bacterial suspensions were dispensed into disposable zeta cells with gold electrodes and allowed to equilibrate for 15 min at 25 °C. The zeta potential for each sample was calculated from the measured value of the electrophoretic mobility using the Smoluchowski equation (18). The complete experiment was carried out twice for each peptide using independently grown cultures.

Atomic Force Microscopy Imaging—In the AFM experiments, images were collected under different conditions. The *E. coli* cells were incubated at 37 °C with 3 μM BP100 and 5 μM pepR for 0.5, 2, and 5 h, and imaged. Bacterial cells incubated at 37 °C for 2 h with 0.3, 3 and 8 μM BP100, and with 0.5, 5, and 20 μM pepR, were also imaged. Control samples were not treated with the peptides. A 100-μl droplet of each test sample was applied onto a poly-L-lysine (PLL) coated glass slide and allowed to stand at 25 °C for 20 min. After deposition, the sample was rinsed 10 times with Milli-Q water, and air-dried at 25 °C. On average, five individual bacterial cells were imaged at high resolution for each peptide concentration and incubation time tested. All experiments were performed with duplicate cultures for each peptide.

The AFM images were acquired using a JPK NanoWizard II (Berlin, Germany) mounted on a Zeiss Axiovert 200 inverted microscope (Göttingen, Germany). Measurements were carried out in intermittent contact mode using uncoated silicon ACL and ACT cantilevers from Applied NanoStructure (Santa Clara, CA). ACL cantilevers had typical resonance frequencies of 190 kHz and a spring constant of 45 N/m, while ACT cantilevers displayed typical frequencies of 300 kHz and a spring constant of 40 N/m. No significant differences in the image acquisition were retrieved whenever ACT or ACL cantilevers were used. Height, error, and phase-shift images were recorded,

and images were line-fitted as required. Height and size information were acquired with the imaging software from JPK.

Surface Roughness Analysis—The data generated from some of the AFM height images were used to calculate the surface roughness of the bacterial cell exterior. Using Gwyddion v2.19 (Czech Metrology Institute, Brno, Czech Republic), the bacterial cell form was estimated through the application of a mean filter to the raw data. Subtraction of the treated image from the original height image generated a flattened representation of the bacterial cell surface; the surface roughness of a selected area of this flattened image was then calculated from the height standard deviation, *i.e.* the root-mean-square value (R_{rms}) of the height distribution in Equation 1,

$$R_{rms} = \sqrt{\sum_{i=1}^{N} \frac{(z_i - z_m)^2}{(N-1)}} \quad \text{(Eq. 1)}$$

where, N is the total number of data points, z_i is the height of the ith point, and z_m is the mean height (19). Roughness values were measured over the entire bacterial cell surface on areas with a fixed size of 125 × 125 nm^2. The average surface roughness of the untreated and AMP-treated *E. coli* cells was then calculated using an unpaired *t* test.

RESULTS

In Vitro Antimicrobial Susceptibility—The antimicrobial activities of BP100 and pepR against *Staphylococcus aureus* (ATCC 25923) and *E. coli* were determined using a modified microtiter broth dilution method (17). Both peptides were found to be inactive against the Gram-positive bacterium *S. aureus*, at concentrations up to 200 μM (data not shown). As such, *S. aureus* was excluded from the rest of the study. Each AMP was observed to inhibit *E. coli* growth to varying degrees. Bacterial growth inhibition by >50% was induced by BP100 using peptide concentrations ranging from 2 to 4 μM (Fig. 1*A*). These values are comparable to those obtained when treating the Gram-negative phytopathogenic bacteria *E. amylovora*, *P. syringae* pv. *Syringae*, and *X. axonopodis* pv. *vesicatoria* with this peptide (13). Peptide concentrations in the range of 2.5–10 μM were necessary for pepR to achieve the same level of inhibition as BP100 (Fig. 1*B*).

Surface Charge Neutralization of E. coli Cells by BP100 and pepR—Zeta potential studies were carried out to monitor the effect of each AMP on the membrane surface charge of *E. coli*. As shown in Fig. 1, *A* and *B*, *E. coli* in the absence of either peptide displayed a zeta potential of −21.9 ± 3.0 mV. Upon the addition of increasing concentrations of BP100, the *E. coli* zeta potential values increased and then stabilized at approximately −0.8 mV (Fig. 1*A*). For pepR, a peptide concentration of 0.63 μM was sufficient to promote negative surface charge neutralization (Fig. 1*B*). At pepR concentrations in the range of 2.5–10 μM, stabilization of the zeta potential at ~9.2 mV was observed (Fig. 1*B*) reflecting an overcompensation in the *E. coli* surface charge. For BP100, the peptide concentration required to induce membrane surface charge neutralization corresponds well to the MIC. In contrast, zero-potential precedes the MIC for pepR.

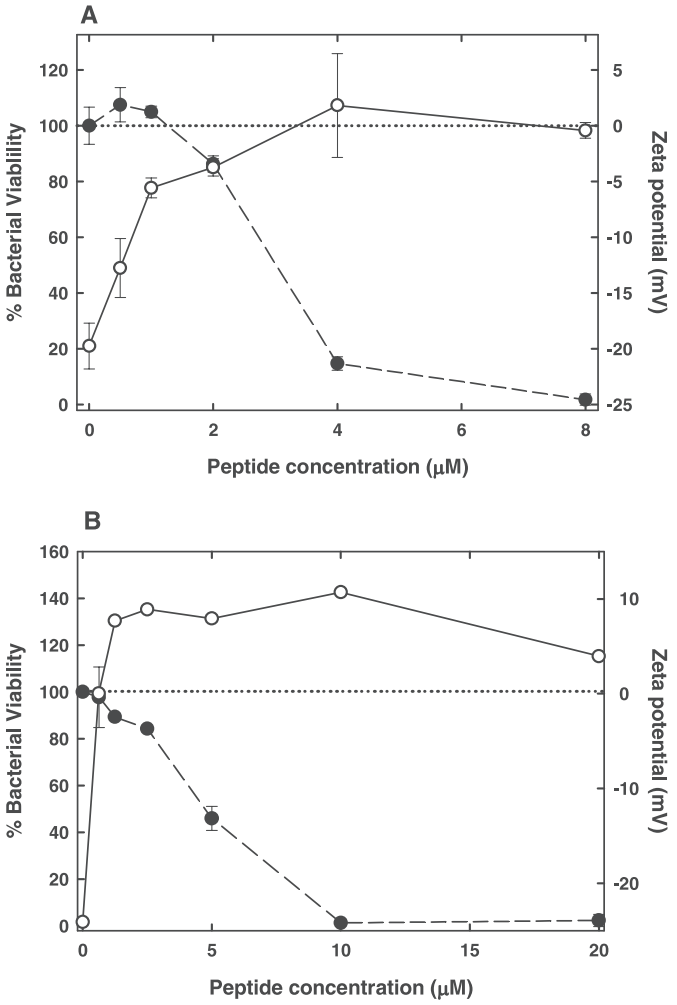

FIGURE 1. **Effect of AMP treatment on the bacterial viability and zeta potential properties of *E. coli*.** *A* and *B*, *E. coli* was treated with BP100 (*A*) and pepR (*B*). Peptide concentrations of 0.5, 1, 2, 4, and 8 μM were tested for BP100, and 0.63, 1.25, 2.5, 5, 10, and 20 μM for pepR. *Dashed lines* (–●–) correspond to the percentage of viable bacterial cells in the presence of increasing peptide concentrations, while the zeta potential is indicated by the *solid lines* (—○—). The *dotted line* both in *A* and *B* indicates a neutral surface net charge, to highlight the peptide concentration range at which *E. coli* surface neutrality and possible overcompensation are achieved. In each case, each value represents the mean of duplicate determinations. *Error bars* represent the S.E.

Atomic Force Microscopy Imaging of Untreated and AMP-treated E. coli Cells—To monitor the effect of AMP treatment on the Gram-negative bacterial cell envelope, AFM images of *E. coli* under various conditions were acquired. Images of a typical untreated *E. coli* bacterium dried in air are presented in Fig. 2. From the lock-in-amplitude image (Fig. 2*A*), it is clear that the membrane surface of the untreated bacterium is reasonably structured. A corrugated surface with no visible pores or ruptures was observed in all the examined cells. A cross-section of the acquired images was used to establish the dimensions of the untreated bacterial cells (Fig. 2, *B* and *C*). The average measured length, width, and height of the untreated cells (n = 23) were 3.42 ± 0.78 μm, 1.18 ± 0.18 μm and 0.22 ± 0.05 μm, respectively. The dimensions of the air-dried *E. coli* cells reported here compare well with those found in the literature (20, 21).

E. coli cells were then treated with the minimum concentration of peptide required to inhibit bacterial growth by 50% for a

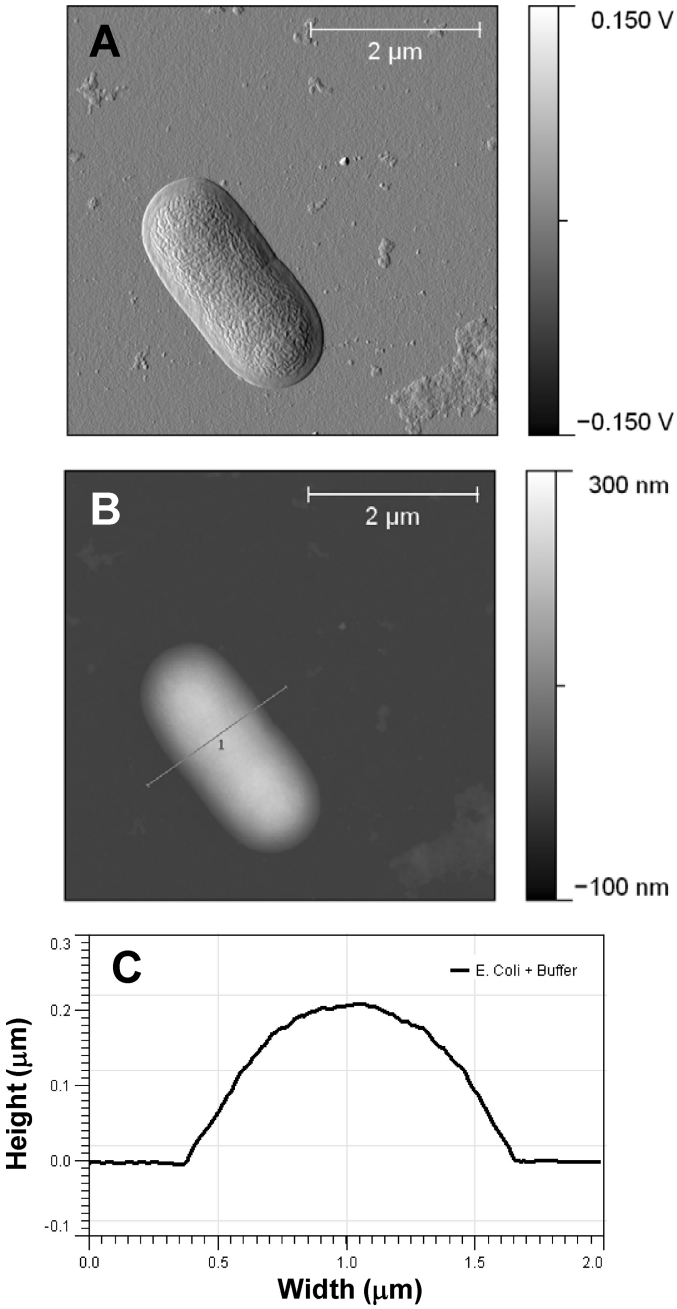

FIGURE 2. **AFM images of an untreated *E. coli* cell dried in air.** *A* and *B*, lock-in-amplitude image (*A*) and topography image (*B*) of *E. coli*. Total scanning area for each image: 4 × 4 μm^2. *C*, cross-section of image indicated in *B*, providing a quantitative measure of the bacterial cell dimensions.

period of 0.5, 2, and 5 h, and imaged. Based on the antimicrobial activity studies, final peptide concentrations of 3 and 5 μM were selected for BP100 and pepR, respectively. Bacteria undergoing no AMP treatment were also imaged at the same time intervals. The images acquired in this study are shown in Fig. 3, presented in three-dimensional orthogonal projection. From Fig. 3, *A* and *B*, it is clear that the untreated *E. coli* cells experienced no morphological changes over the period of 2 h. The typical rod-shaped structure was preserved, and the surface topography was comparable to that of the untreated cells imaged immediately after sample preparation. After 5 h of incubation, however, an alteration in the morphology of the untreated cells was observed (Fig. 3*C*). Keeping *E. coli* in the nutrient-free buffer led to the eventual starvation of the bacterial cells and the consequent shriveling of their overall structure. The nature of the surface corrugation detected here is markedly different from that of the bacterial cells incubated with either AMP (Fig. 3, *D–I*).

The effect of BP100 and pepR on *E. coli*, following incubation for the different time intervals, was comparable (Fig. 3, *D–I*). In all cases, the treated bacterial cells retained their rod-like form. However, changes in the membrane surface corrugation could already be distinguished for the bacterial cells incubated for 0.5 h with either 3 μM BP100 (Fig. 3*D*) or 5 μM pepR (Fig. 3*G*). A minor collapse in the outer membrane of the bacterial cell treated with BP100 was evident (see highlighted region in Fig. 3*D*). Also, in the case of pepR, treatment seemed to induce membrane blebbing (see highlighted region in Fig. 3*G*). Exposure of the cells to either AMP for 2 h or longer led to greater membrane disruption (Fig. 3, *E*, *F*, *H*, and *I*). Broadly speaking, the action of both BP100 and pepR over time resulted in a collapse of the bacterial envelope, particularly at the septal region. This was associated with the formation of vesicle-like structures on the membrane surface. Some leaked contents and debris could also be detected around the partially disintegrated cells (Fig. 3, *E* and *I*). The events described here were observed for almost all cells imaged under the same conditions.

The effect of AMP concentration on bacterial cell morphology was also assessed by AFM, as shown in Fig. 4. *E. coli* cells were incubated for 2 h with 0.3, 3, and 8 μM BP100 and 0.5, 5, and 20 μM pepR. From all the acquired images, it is clear that the typical rod-shaped structure of the *E. coli* cells was maintained following peptide treatment. However, characteristic phenomena associated with the exposure of *E. coli* to increasing concentrations of either BP100 or pepR were detected (Fig. 4, *A–F*). Exposure of the cells to 0.3 μM BP100 (Fig. 4*A*) and 0.5 μM pepR (Fig. 4*D*) already induced minor perturbations on the bacterial envelope in comparison to the untreated cells (Fig. 3*B*). Membrane blebbing and a minor collapse at the apical end of the bacterial envelope were observed. Upon incubation of *E. coli* with 3 μM BP100 (Fig. 4*B*), a pronounced collapse in the mid-region of the envelope was detected. This was accompanied by the leakage of the cytoplasm contents of the bacterial cell. A similar event was registered when treating *E. coli* cells with 8 μM BP100 (Fig. 4*C*). Only here a copious amount of fluid leaked contents and debris around the apical and septal regions of the dividing cell was released. For pepR, treatment of the bacterial cells with 5 μM (Fig. 4*E*) and 20 μM (Fig. 4*F*) peptide concentrations resulted in comparable alterations in the membrane surface. In both cases, the formation of vesicle-like structures on the membrane surface was visible. For all the AMP-damaged *E. coli* cells imaged here, different combinations of the above-described phenomena were recorded.

Surface Roughness Analysis of the AFM Imaged, Untreated, and AMP-treated E. coli Cells—To quantify the damage exerted by each AMP, the roughness of the treated *E. coli* bacterial cell surface was measured. The AFM concentration-dependent studies showed that the treatment of *E. coli* with either AMP at concentrations equivalent to the MICs was sufficient for the complete disruption of the bacterial cell envelope.

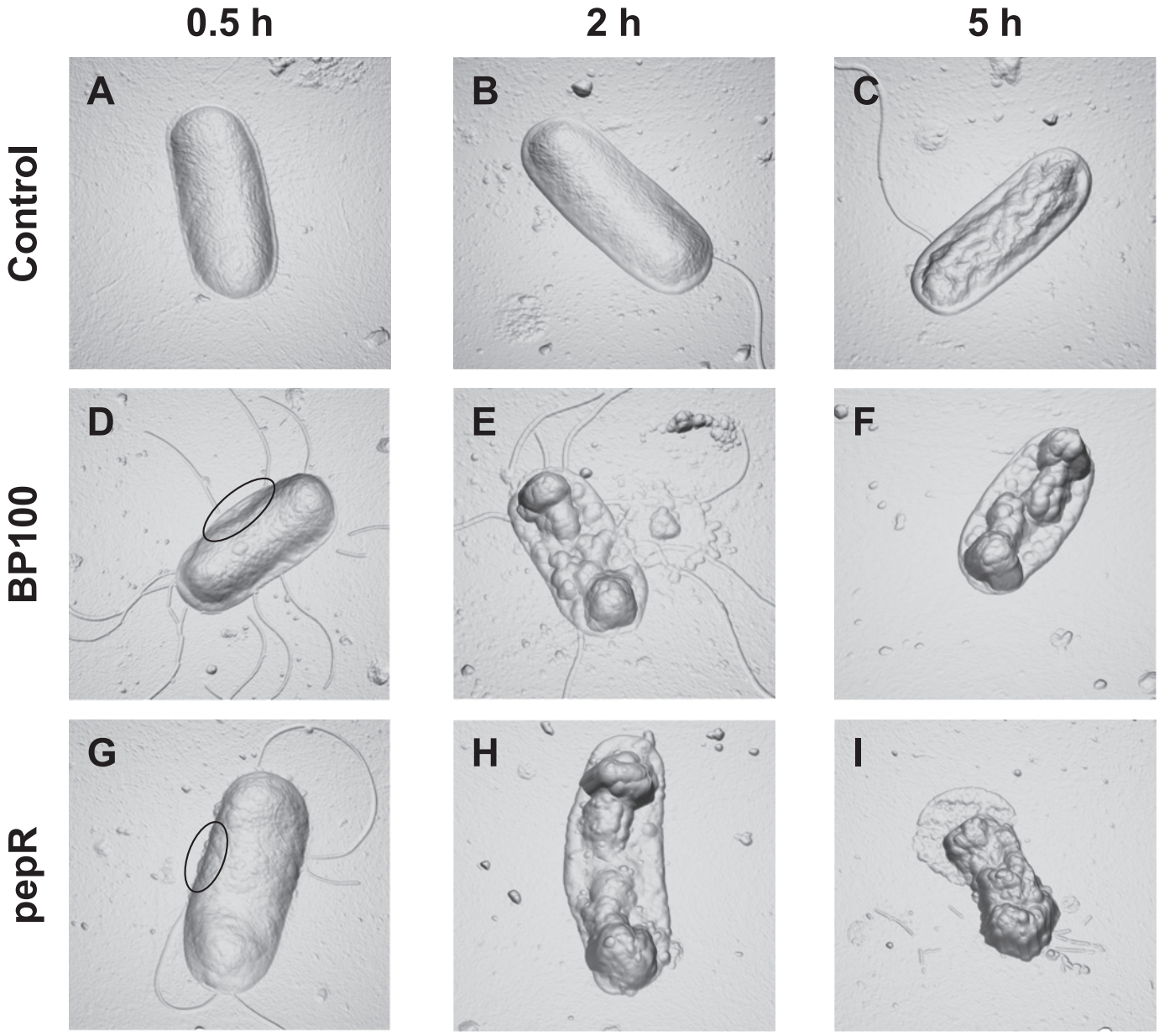

FIGURE 3. **Time dependence of AMP effects on *E. coli* imaged by AFM.** *A–I*, three-dimensional orthogonal projection images (derived from the height data) of untreated *E. coli* cells (*top row*), and *E. coli* cells treated with 3 μM BP100 (*middle row*), and 5 μM pepR (*bottom row*). Images were acquired following the treatment of the bacterial cells for 0.5 h (*first column*), 2 h (*second column*), and 5 h (*third column*). Total scanning area for each image: 4×4 μm^2. See the text for a description of the highlighted areas.

Therefore, the surface roughness measurements were only compared for the bacterial cells treated with AMP at concentrations below and at MICs. Surface roughness measurements of the untreated cells served as a control.

The typical procedure applied to each AFM image assessed is illustrated in Fig. 5. In essence, the original AFM height image (Fig. 5*A*) was subtracted from the equivalent treated height image (Fig. 5*B*). The resultant flattened image (Fig. 5*C*) was then analyzed by calculating the R_{rms} of the height distribution over the entire bacterial cell surface on areas with a fixed size of 125×125 nm^2 (Fig. 5*D*). Fig. 6 shows the comparison of the average surface roughness calculated for the untreated and the AMP-treated *E. coli* cells. The average surface roughness of the *E. coli* cells treated with either 0.3 μM BP100 (2.3 ± 0.3 nm) or 0.5 μM pepR (2.3 ± 0.2 nm) was comparable to that recorded for the untreated cells (2.5 ± 0.3 nm). The measured surface roughness of the cells treated with 3 μM BP100 and 5 μM pepR were 8.4 ± 6.0 nm and 10.8 ± 3.5 nm, respectively. Clearly, the use of either AMP at concentrations below MICs induced minor detectable alterations in the bacterial surface. The treatment of *E. coli* with BP100 and pepR at the respective MIC values, however, resulted in a dramatic increase in the bacterial surface roughness. Here, the damaging effect exerted by pepR was greater than that exerted by BP100.

DISCUSSION

Biophysical studies have previously been employed to explore the mode of action of BP100 (14). In these studies, the

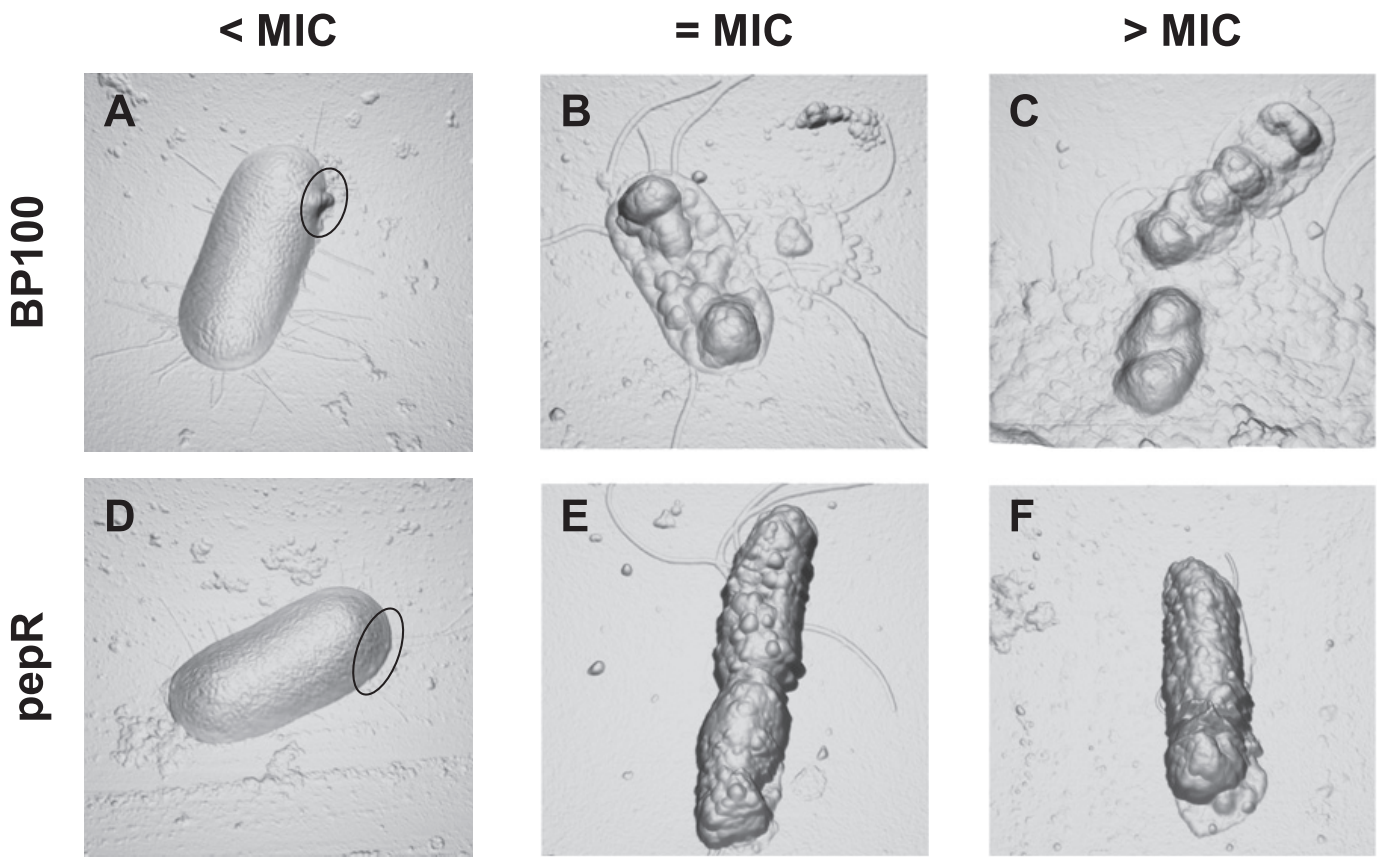

FIGURE 4. **Concentration dependence of AMP effects on *E. coli* imaged by AFM.** *A–F*. Three-dimensional orthogonal projection images (derived from the height data) of *E. coli* cells incubated for 2 h with either BP100 (*top row*) or pepR (*bottom row*) using concentrations below, at, and above MIC values. For BP100, 0.3 μM (*A*), 3 μM (*B*), and 8 μM (*C*) concentrations were tested, while for pepR 0.5 μM (*D*), 5 μM (*E*), and 20 μM (*F*) concentrations were used. Total scanning area for each image: 4 × 4 μm^2. See the text for a description of the highlighted areas.

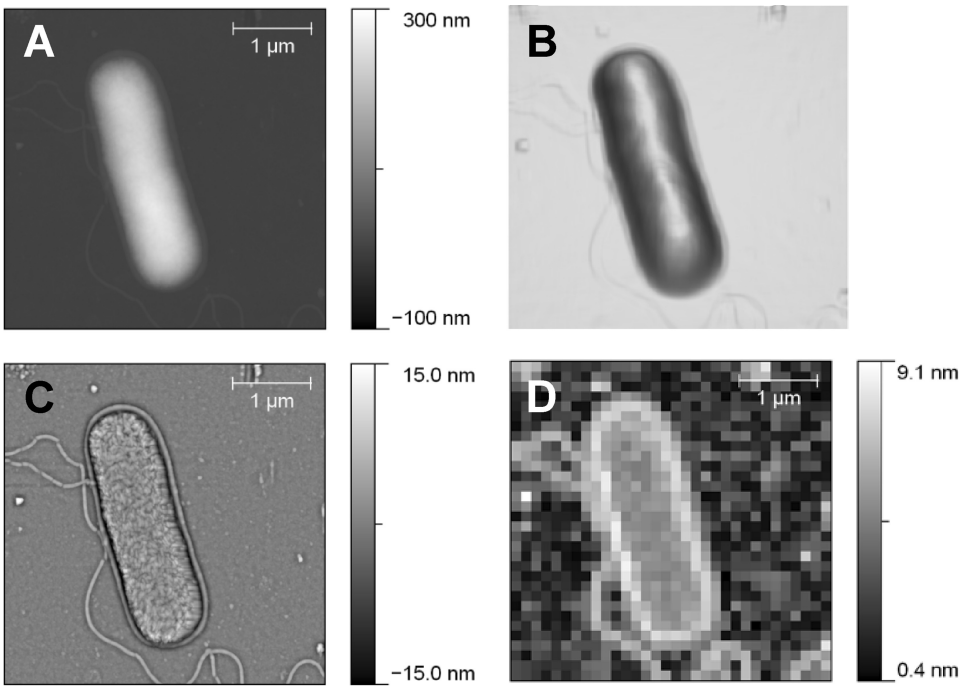

FIGURE 5. **Surface roughness analysis procedure applied to the AFM images.** *A–D*, originally acquired AFM height image of *E. coli* (*A*) was treated, through the application of a mean filter, to estimate the bacterial cell form (*B*). The treated image data (*B*) was then subtracted from the original height image data (*A*). The resultant flattened image of the bacterial cell surface (*C*) was then analyzed by measuring the root-mean-square value (R_{rms}) of the height distribution over the entire bacterial cell surface, on areas with a fixed size of 125 × 125 nm^2 (*D*).

binding affinity and damaging effect of BP100 on phospholipid bilayers having lipid compositions similar to that of the bacterial cytoplasmic membrane were explored. In addition to the ability of this peptide to permeabilize and translocate the model bacterial membrane, surface charge neutralization upon membrane saturation was detected. The peptide concentrations required for saturation and consequently neutralization to occur (14) were found to be in the range of that required for microbial inhibition (13). Clearly, these closely coupled events provide some insight into the antimicrobial mechanism adopted by BP100. Although these concepts have already been extended to other AMPs (reviewed in Ref. 7), there is still a need to draw parallels between the biophysical and biological studies. In the present study, a correlation between antimicrobial susceptibility and bacterial surface charge neutralization as exerted by

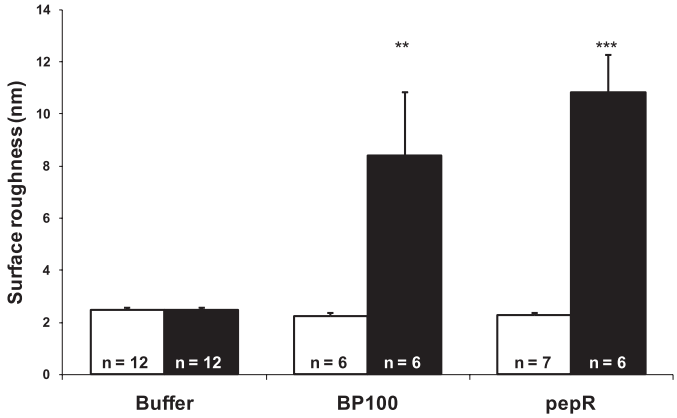

FIGURE 6. ***E. coli* cell surface topography analysis.** The average surface roughness of the untreated *E. coli* cells, and the *E. coli* cells treated with either BP100 or pepR were compared. The AFM height images evaluated for BP100 were those of *E. coli* treated with either 0.3 μM (below MIC) or 3 μM (at MIC) concentrations. For pepR, the height images evaluated were those of *E. coli* treated with either 0.5 μM (below MIC) or 5 μM (at MIC) concentrations. The surface roughness of *E. coli* when treated with either AMP using concentrations equivalent to MIC values was significantly enhanced: **, $p < 0.05$ for 3 μM BP100 when compared with either the untreated cells or the cells treated with 0.3 μM BP100; ***, $p < 0.0005$ for 5 μM pepR when compared with either the untreated cells or the cells treated with 0.5 μM pepR. *Error bars* indicate the S.E.

either BP100 or pepR on *E. coli* was investigated. AFM imaging was also used to gain some insights into the mode of action of each AMP against *E. coli*, at an atomic level.

Both BP100 and pepR were found to be effective antimicrobial agents against *E. coli*, inhibiting the growth of this Gram-negative bacterium at micromolar concentrations. Inhibition occurred to an equivalent extent for both peptides, with pepR being only slightly more effective at lower peptide concentrations. For the BP100-treated *E. coli* cells, the MICs recorded were comparable to those previously reported for *E. amylovora*, *P. syringae* pv. *Syringae*, and *X. axonopodis* pv. *vesicatoria* (13), as well as the theoretically determined values (14).

Having established the MICs for each peptide, zeta potential studies were performed under the equivalent experimental conditions. In doing so, characterization of the bacterial surface following the addition of either cationic AMP at MICs was made possible. In the absence of peptide, the *E. coli* surface displayed a zeta potential of -21.9 ± 3.0 mV. This negative surface net charge originates from the negative lipids and lipopolysaccharide (LPS) molecules present in the outer leaflet of the Gram-negative bacteria outer membrane (18, 20). Analysis of the electrostatic properties of the *E. coli* surface by zeta potential measurement, after incubation with either AMP, revealed significant differences between both peptides. The observed behavioral differences recorded for each AMP can be rationalized on the basis of the peptide and membrane properties. For BP100, the surface charge of the bacteria was neutralized when using concentrations at, and above, the MIC (*i.e.* >2 μM). This corresponds well to the biophysical data, where surface neutralization of the model bacterial membrane was induced by equivalent BP100 concentrations at the saturation state (14). The postulated saturation-triggered antimicrobial mechanisms adopted by BP100 (14) thus appear to be connected to the neutralization of the bacterial surface when using peptide concentrations equivalent to MICs. In biological systems, surface neutralization can largely be attributed to the balance in electrostatic interactions between the positive charges (mainly lysine and arginine side chains) of the peptides with the negatively charged groups (mainly phosphates and carboxylates) of LPS. For BP100 (+6 at pH 7.4) in a model bacterial membrane, it has been proposed that one peptide molecule interacts with 5.6 negatively charged phospholipid molecules at saturation, thereby inducing neutralization (14). This phenomenon more than likely accounts for BP100 behavior when treating *E. coli* cells with the peptide at MIC.

For pepR, surface neutralization of *E. coli* occurred at peptide concentrations below MIC values (0.63 μM). In fact, a charge overcompensation was registered in the zeta potential measurements when treating *E. coli* with pepR at concentrations above 1.25 μM. Mechanisms other than just surface neutralization seem to be present in the case of pepR. Relative to BP100, pepR is considerably more basic and positively charged (+12 at pH 7.4). The interaction of this peptide with *E. coli* at low concentrations (*i.e.* below MIC) can be attributed, at least initially, to electrostatics. Several studies investigating the interaction of cationic AMPs with model bacterial membranes have shown that an overcompensation in zeta potential at high peptide concentrations is associated with membrane insertion via hydrophobic interactions (22–24). A similar trend was also reported for the interaction of the cationic peptide $rBPI_{21}$ with LPS aggregates (24). The overcompensation in *E. coli* zeta potential at high pepR concentrations (≥MICs) may indicate: 1) that hydrophobic interactions contribute to membrane interaction in addition to electrostatic attraction, or 2) not all positive charges of pepR contribute to electroneutralization. The relatively large size of pepR, as well as the large majority of charged/polar residues within the peptide, makes it unlikely that all its charges will be able to simultaneously come into contact with the bacterial surface. Thus, the observed zero in zeta potential at low concentrations of pepR may not correspond to the actual neutralization of the surface but rather its masking by unbound charges. This interpretation conciliates the zeta potential results of pepR with the MIC-neutralization correlation hypothesis. In any case, the existence of an inherent neutralization-mediated killing mechanism employed by either AMP is not necessarily implied.

To gain further insights into these MIC-associated events, AFM images of the *E. coli* cells under varying conditions were acquired. The use of the cationic polymer PLL as an adhesion molecule for bonding bacteria to surfaces prior to AFM imaging has been questioned (25), in part due to its potential antimicrobial activity (26, 27). However, it has been demonstrated that the use of this method for imaging bacteria in their native state does not affect the properties of the bacterial membrane surface (28, 29). Bacteria can also be imaged in an air-dried state, as this enables the high-resolution imaging of their surface morphology (28, 30, 31). For this reason, the bacterial cells imaged in this study were immobilized onto glass slides functionalized with PLL and allowed to air-dry. Overall, satisfactory and informative AFM images of the untreated and AMP-treated bacterial cells were acquired, revealing detailed information on the membranolytic properties of both BP100 and

pepR. Nonetheless, it should be borne in mind that, due to the deposition and washing protocols, free debris resulting from cell disruption are partially eliminated.

The AFM results presented in this study clearly demonstrate the time- and concentration-dependent antimicrobial activity of both BP100 and pepR. Intricate details of the damage sustained by the *E. coli* cells following AMP treatment under the different conditions were revealed. During the initial stages of treatment, where cells were incubated with peptide either for short periods of time (0.5 h) or using low peptide concentrations (below MICs), minor changes in the outer membrane of the bacterial cell envelope were induced. The appearance of blebs at the bacterial surface, as well as the slight collapse in the outer membrane, already pointed to the interaction of either AMP to the negatively charged LPS outer layer. The formation of vesicle-like structures, as well as the alterations in surface roughness, observed in the *E. coli* cells exposed to either BP100 or pepR for longer time periods (≥2 h) and at higher peptide concentrations (≥MICs) confirmed this. Previous studies have demonstrated that an increase in surface roughness is a direct consequence of AMP incorporation into the LPS-containing outer membrane (21, 30, 32, 33). It has also been shown that release of LPS-containing vesicles and even autolytic reactions are possible outcomes of such interactions (21, 30, 32). When exposing *E. coli* to either BP100 or pepR under extreme conditions (*i.e.* long exposure time, ≥2 h; high peptide concentrations, ≥MICs), a collapse of the outer membrane at the septal region was generally observed. In some images, a release of cytoplasmic content was also detected. These phenomena may be explained by taking into account that cardiolipin, a negatively charged phospholipid, is generally located at the apical and septal regions of the *E. coli* inner membrane (34), and that both BP100 and pepR are highly cationic. Furthermore, BP100, which displays a high affinity toward negatively charged phospholipids, is known to induce vesicle permeabilization at high peptide/lipid ratios (14). It is therefore likely that treatment of *E. coli* with either AMP for long periods of time, or when using high concentrations, could result in an accumulation of peptide at either the apical or septal regions. When a threshold peptide concentration is reached in these regions, membrane disruption may occur, thereby initiating cell leakage. Similar observations have been reported for the cationic AMPs magainin 2, melittin, PGLa, and Sushi 3 (21, 32). Based on the nature of such alterations, the adoption of a carpet-like or detergent-like mechanism (9) *in vivo* by the two AMPs investigated here seems to be likely.

Combining the antimicrobial susceptibility, zeta potential and AFM data, the closely coupled events leading to *E. coli* cell death after AMP treatment can thus be summarized as follows. At peptide concentrations below MIC, an association of the cationic AMP with the negatively charged LPS molecules in the bacterial outer membrane occurs. For BP100, this event involves an initial electrostatic interaction between the peptide and the LPS molecules and a gradual increase of the membrane surface charge. In contrast, the electrostatic association of pepR to the LPS outer layer prompts an almost immediate net neutralization of the membrane surface charge. At an initial stage and at low extents of peptide binding, minor changes in the bacterial cell envelope are provoked (*e.g.* bleb formation and slight collapse in the outer membrane). Treatment of *E. coli* with either AMP at, and above the MIC, brings about further membrane alterations (*e.g.* increase in surface roughness and formation of vesicle-like structures). After the permeabilization of the outer membrane and cell envelope, each AMP interacts with the negatively charged phospholipids of the bacterial inner membrane. In the case of BP100, these events are associated with saturation (14) and, consequently, neutralization of the membrane. For pepR, events beyond electrostatic equivalence prompt peptide binding to the inner membrane. The final stages leading to *E. coli* cell death, as evidenced by the release of cytoplasmic content, involve the disruption of the inner membrane by either AMP.

The differences in the MIC values of the two peptides may also be closely related to their charge behavior. It has been proposed that threshold events that lead to cell death (35) depend on the strain imposed on the cell membrane due to peptide-induced thinning. The reaching of such thresholds requires that peptide molecules become concentrated in the membrane despite an intrinsic repulsion between them as their density increases. The driving forces that overcome this repulsion are the electrostatic and hydrophobic peptide-membrane interactions, which also result in the typically high membrane binding affinities of AMPs (7). Bacterial surface charge neutralization by pepR occurs at very low peptide concentrations, which is a likely consequence of the high cationicity of the peptide. From neutralization onward, only the hydrophobic interactions will be left to draw more peptide molecules to the membrane (the zeta potential increasing above 0 mV; Fig. 1*B*) and across the disruption threshold. With a weaker driving force to bind the membrane, larger amounts of peptide are eventually required for the threshold to be reached, which translates into a higher MIC. Ultimately, too high a cationic charge on an AMP may actually compromise its activity. This concept may in fact account for the observed lack of antibacterial activity reported for some of the cecropin A-melittin hybrid peptides (*e.g.* BP16, +9 at pH 7.4) developed by Ferre *et al.* (36).

Based on the data presented in this work, insights into the events leading to *E. coli* cell death after treatment with either BP100 or pepR were gained. This was achieved through the unconventional approach of bridging the microbiological properties of each AMP with some of their respective biophysical characteristics. Firstly, the question of a neutralization-mediated killing mechanism adopted by either AMP was addressed. Exploration of this concept using a standard antimicrobial activity assay and zeta potential studies demonstrated a clear correlation linking the MICs of each AMP to corresponding alterations in the *E. coli* surface charge. More specifically, neutralization of the bacterial surface was detected when treating *E. coli* with peptide concentrations close to MIC values. Visual insights into these MIC-associated events were then sought. The acquisition of AFM images of *E. coli* cells treated with either BP100 or pepR under varying conditions illustrated the time- and concentration-dependent antimicrobial action of both AMPs. Taken together, the biological and biophysical data acquired in this study clearly point to a critical AMP concen-

tration, equivalent to MIC values, being necessary for *E. coli* membrane disruption to occur.

REFERENCES

1. Zasloff, M. (2002) *Nature* **415,** 389–395
2. Brogden, K. A. (2005) *Nat. Rev. Microbiol.* **3,** 238–250
3. Yeaman, M. R., and Yount, N. Y. (2003) *Pharmacol. Rev.* **55,** 27–55
4. Jenssen, H., Hamill, P., and Hancock, R. E. W. (2006) *Clin. Microbiol. Rev.* **19,** 491–511
5. Hancock, R. E., and Chapple, D. S. (1999) *Antimicrob. Agents Chemother.* **43,** 1317–1323
6. Huang, H. W. (2000) *Biochemistry* **39,** 8347–8352
7. Melo, M. N., Ferre, R., and Castanho, M. A. (2009) *Nat. Rev. Microbiol.* **7,** 245–250
8. Ludtke, S. J., He, K., Heller, W. T., Harroun, T. A., Yang, L., and Huang, H. W. (1996) *Biochemistry* **35,** 13723–13728
9. Bechinger, B., and Lohner, K. (2006) *Biochim. Biophys. Acta* **1758,** 1529–1539
10. Leontiadou, H., Mark, A. E., and Marrink, S. J. (2006) *J. Am. Chem. Soc.* **128,** 12156–12161
11. Oren, Z., and Shai, Y. (1998) *Peptide Science* **47,** 451–463
12. Andreu, D., Ubach, J., Boman, A., Wåhlin, B., Wade, D., Merrifield, R. B., and Boman, H. G. (1992) *FEBS Lett.* **296,** 190–194
13. Badosa, E., Ferre, R., Planas, M., Feliu, L., Besalú, E., Cabrefiga, J., Bardají, E., and Montesinos, E. (2007) *Peptides* **28,** 2276–2285
14. Ferre, R., Melo, M. N., Correia, A. D., Feliu, L., Bardají, E., Planas, M., and Castanho, M. (2009) *Biophys. J.* **96,** 1815–1827
15. Ma, L., Jones, C. T., Groesch, T. D., Kuhn, R. J., and Post, C. B. (2004) *Proc. Natl. Acad. Sci. U. S. A.* **101,** 3414–3419
16. Fields, G. B., and Noble, R. L. (1990) *Int. J. Pept. Protein Res.* **35,** 161–214
17. Wiegand, I., Hilpert, K., and Hancock, R. E. (2008) *Nat. Protocols* **3,** 163–175
18. Domingues, M. M., Santiago, P. S., Castanho, M. A., and Santos, N. C. (2008) *J. Pept. Sci.* **14,** 394–400
19. Girasole, M., Pompeo, G., Cricenti, A., Congiu-Castellano, A., Andreola, F., Serafino, A., Frazer, B. H., Boumis, G., and Amiconi, G. (2007) *Biochim. Biophys. Acta* **1768,** 1268–1276
20. Amro, N. A., Kotra, L. P., Wadu-Mesthrige, K., Bulychev, A., Mobashery, S., and Liu, G. Y. (2000) *Langmuir* **16,** 2789–2796
21. Meincken, M., Holroyd, D. L., and Rautenbach, M. (2005) *Antimicrob. Agents Chemother.* **49,** 4085–4092
22. Andrä, J., Koch, M. H., Bartels, R., and Brandenburg, K. (2004) *Antimicrob. Agents Chemother.* **48,** 1593–1599
23. Den Hertog, A. L., Wong Fong Sang, H. W., Kraayenhof, R., Bolscher, J. G., Van't Hof, W., Veerman, E. C., and Nieuw Amerongen, A. V. (2004) *Biochem. J.* **379,** 665–672
24. Domingues, M. M., Castanho, M. A., and Santos, N. C. (2009) *PLoS One* **4,** e8385
25. Colville, K., Tompkins, N., Rutenberg, A. D., and Jericho, M. H. (2009) *Langmuir* **26,** 2639–2644
26. Conte, M., Aliberti, F., Fucci, L., and Piscopo, M. (2007) *World J. Microbiol. Biotechnol.* **23,** 1679–1683
27. Yoshida, T., and Nagasawa, T. (2003) *Appl. Microbiol. Biotechnol.* **62,** 21–26
28. Bolshakova, A. V., Kiselyova, O. I., Filonov, A. S., Frolova, O. Y., Lyubchenko, Y. L., and Yaminsky, I. V. (2001) *Ultramicroscopy* **86,** 121–128
29. Schaer-Zammaretti, P., and Ubbink, J. (2003) *Ultramicroscopy* **97,** 199–208
30. da Silva, A., Jr., and Teschke, O. (2005) *World J. Microbiol. Biotechnol.* **21,** 1103–1110
31. Ubbink, J., and Schär-Zammaretti, P. (2005) *Micron* **36,** 293–320
32. Li, A., Lee, P. Y., Ho, B., Ding, J. L., and Lim, C. T. (2007) *Biochim. Biophys. Acta* **1768,** 411–418
33. Matsuzaki, K., Sugishita, K., and Miyajima, K. (1999) *FEBS Lett.* **449,** 221–224
34. Mileykovskaya, E., and Dowhan, W. (2000) *J. Bacteriol.* **182,** 1172–1175
35. Huang, H. W. (2009) *Biophys. J.* **96,** 3263–3272
36. Ferre, R., Badosa, E., Feliu, L., Planas, M., Montesinos, E., and Bardají, E. (2006) *Appl. Environ. Microbiol.* **72,** 3302–3308